Suppressing supercooling in magnesium nitrate hexahydrate and evaluating corrosion of aluminium alloy container for latent heat storage application

Pavla Honcova[1], Radim Pilar[1], Vladimir Danielik[2], Peter Soska[2], Galina Sadovska[1*] and Daniel Honc[3]

[1]*Department of Inorganic Technology, Faculty of Chemical Technology, University of Pardubice, Doubravice 41, 53210 Pardubice, Czech Republic*

[2]*Department of Inorganic Technology, Slovak University of Technology in Bratislava, Bratislava, Slovakia*

[3]*Department of Process Control, Faculty of Electrical Engineering and Informatics, University of Pardubice, Cs. Legii Sq. 565, 53002 Pardubice, Czech Republic*

**corresponding author: galina.sadovska@upce.cz*

DOI 10.1007/s10973-017-6334-0

1. Introduction

Converting the solar irradiation, approximately 1 kWh m^{-2} per year in Central Europe, into electricity or storing it in the form of a thermal energy represents the future trends in affordable and clean energy sources. The latter uses different materials, for example natural resources such as water, stones, and oils, or special mixtures of organic and inorganic substances, to store the solar energy [1]. The energy can be stored either as sensible or latent heat during chemical reactions or phase transitions.

Hydrated salts have often been tested as the active materials for the phase-change energy storage because the transitions occur in appropriate temperature range, and the high enthalpies of the transitions, typically from 100 to 300 J g^{-1} results in efficient energy accumulation [2]. The other requirements on the hydrated salt are congruent melting and minimized supercooling, $\Delta T = T_m - T_{cr}$, where T_m is the melting temperature, and T_{cr} is the crystallization temperature. The former results decreased storage efficiency because of the formation of lower hydrated salt making the process almost irreversible. Supercooling is observed on cooling when the equilibrated liquid of the melted salt does not solidify at the freezing point and remains in a supercooled liquid state; ΔT around 20 K [3], and even above 40 K [4] has been observed, and this does not allow heat releasing. Supercooling can be reduced, or complete avoided, by adding nucleation agents, typically crystals from the group of the stable salts, or using admixture with appropriate hydrated salt [2]. The focus of this paper is to study suppression of supercooling in magnesium nitrate hexahydrate (MNH).

MNH of the molecular weight M = 256.41 g mol^{-1} crystallizes in the monoclinic system with respectively density of 1.636 g cm^{-3} at T = 298.15 K and 1.55 g cm^{-3} at T = 368.15 K, and the thermal conductivity of 0.611 W m^{-1} K^{-1} (T = 310 K) and 0.490 W m^{-1} K^{-1} (T = 369.15 K) for solid and liquid states [5]. Differential-scanning calorimetry (DSC) traces on MNH heating show two separate endothermic phase transitions. MNH undergoes a solid-solid phase transition around between 344.0–346.15 K with the enthalpy change of $\Delta_{trs}H$ = 12.1–12.5 J g^{-1} [5–7], and then melts in temperature interval of 362.2–368.15 K with the heat of fusion, $\Delta_{fus}H$, varying from 150.2 to 166.9 J g^{-1} [5–15]. The detailed study of MHN

thermal properties, including temperature dependence of heat capacity, can be found in Refs. [7,13,16,17].

Lane [2] tested 11 isotypic nucleating agents, mainly sulphates and 18 non-isostructural salts, to suppress supercooling in MNH. The freeze test results of the role of nucleating agents, presented in the reference, are difficult to compare because different number of cycles 3–68 were used. Non-isostructural salts, predominantly Sr^{2+}, Ca^{2+}, Mg^{2+} and Ba^{2+} carbonates, hydroxides, and oxides were identified as promising additives.

Corrosion of metallic materials in nitrate hydrates has only been studied in a few papers [18–21]. Cabeza *et al.* [18] tested the corrosive properties of zinc nitrate hexahydrate upon short-term 14 days contact with aluminium and cooper, and alloys such as stainless steel, brass, and steel. They observed that zinc nitrate hexahydrate is extremely corrosive to brass (Ms58 Flach), steel (1.0345), aluminium (EN AW 2007), and copper (E-Cu 57). Stainless steel (1.4301) was the only material resistant to corrosion in zinc nitrate hexahydrate. The same conclusions were reached, by Cabeza *et al.* [19], after prolong contact of 75 days.

Nagano *et al.* [20] studied material compatibility of magnesium nitrate hexahydrate with the addition of magnesium chloride hexahydrate (10 wt%) in contact with six metallic containers (copper, carbon steel, brass, two types of stainless steel S30403 and S31603, and aluminium). Each metallic sample was placed inside a glass tube at a constant temperature of 368.15 K for 90 days. Copper, steel, and brass experienced strong corrosion with the corrosion weight loss of 106 mg cm^{-2} $year^{-1}$, 82 mg cm^{-2} $year^{-1}$, and 28 mg cm^{-2} $year^{-1}$, respectively. Stainless steels showed small corrosion weight losses (1.03 mg cm^{-2} $year^{-1}$ and 0.16 mg cm^{-2} $year^{-1}$), but almost whole surface area of S30403 and a small portion of S31603 were covered with a dotted red-brown rust. The corrosion weight loss of aluminium reached the value of 0.04 mg cm^{-2} $year^{-1}$; it is the only metal not corrosively affected by the salt.

Moreno *et al.* [21] studied the corrosive properties of several phase-change materials (PCMs) including zinc nitrate tetrahydrate. Four sample containers were tested: copper, stainless steel 316, carbon steel, and aluminium. Corrosion rate, salt precipitation and bubbles formation were tested after 1, 4 and 12 weeks. Stainless steel was the only alloy compatible with zinc nitrate tetrahydrate. Copper, aluminium and carbon steel suffered strong corrosion losses after being in contact with the salt for 12 weeks.

The focus of this paper is to test the influence of different nucleation agents in wider range of concentration ratio on supercooling in magnesium nitrate hexahydrate. Long-term stability of the promising composition during 50 heating/cooling cycles is tested, and the corrosion properties of the salt in an aluminium alloy-based container are studied.

2. Experimental part

Magnesium nitrate hexahydrate ($Mg(NO_3)_2.6H_2O$, – MNH) (Lachner, 99.0% purity) was of an analytical reagent grade and stored in a fridge. The exact amount of the hydrate water was measured by a chelatometric titration; the average value was 6.07 moles. The crystallographic structure was checked by X-ray diffraction analysis (Bruker AXE) performed at 298.15 K, and the thermal properties of the salt were characterised using a thermogravimeter with a differential-thermal analyser DTA-TG (STA Jupiter 449, Netzsch). Results of the both analyses were similar to that published in [7].

Calorimetric measurements were done using a DSC Pyris 1 (Perkin-Elmer, USA) with an Intracooler 2P. The calorimeter was calibrated using T_m of pure metals (Hg, Ga, In, Sn, Pb and Zn), and the enthalpy change was calibrated using the heat of fusion, $\Delta_{fus}H$, of indium. The experiments were carried out in temperature range of 273–383 K with heating and cooling rates of 10 K min^{-1} in the atmosphere of dry nitrogen (a flow rate of 20 cm^3 min^{-1}). Mixtures of MNH with selected additive (nucleation agent) were prepared by

weighting the appropriate amount of components into agate mortar (approximately 0.5 g of the mixture), and mixed for 3 minutes. Samples for DSC were prepared by weighting the prepared mixtures (approximately 12 mg) into an aluminium pan, which was then closed. The determination of accumulated heat energy includes the sensible part of the heat capacity and the heat of fusion or the enthalpy of phase change.

Thermal stability of MNH was studied during 75 heating/cooling cycles (75 cycles of melting/crystallization processes, see Fig. 1). The extrapolation of the onset temperatures was used to read the melting, T_m, and crystallization, T_{cr}, temperatures (evaluation is illustrated in Fig. 1), and the heat of fusion $\Delta_{fus}H$, and the heat of crystallization, $\Delta_{cr}H$, were calculated from the area of DSC peaks. Nucleating agents AlO(OH) (>94%, Sasol), BaO (97%, Aldrich), BaO_2 (95%, Fluka), $Ba(OH)_2.8H_2O$ (≥98%, Lachner), $BaCO_3$ (≥99%, Penta), CaO (≥97%, Penta), $Ca(OH)_2$ (≥96%, Lachner), $CaCO_3$ (≥99%, Penta), MgO (≥98%, Penta), $Mg(OH)_2$ (≥99%, Sigma-Aldrich), $MgCO_3$ (basic, 84%, Lachner), $Sr(OH)_2$ (≥94%, Aldrich), and $SrCO_3$ (99%, Penta) all in analytical purity were tested to supress supercooling observed in MNH. Initially, MNH was mixed with 1 wt% of each nucleating agent, and influence on supercooling was tested during 4 heating/cooling cycles. On the base of these quick tests, the promising mixtures containing 1 wt% of the selected agent were tested during 50 temperature cycles; additional mixtures of MNH with 0.5 and 2 wt% of the selected nucleating agent were tested as well.

The corrosion tests were for two parallel samples of aluminium alloy (EN AW 1050A). The aluminium tubes (dimensions: an outer diameter of 10.0 mm, an inner diameter 8.0 mm and a length of 10 mm) were placed onto a small glass pedestal in a sealed flask (a volume of 400 ml) filled with the corrosive liquid. The pedestal ensures proper contact between the alloy and the liquid even when it partially solidifies. The flasks were immersed in a water bath preheated to 363.15 K, which is chosen to be close to the melting point of the corrosive liquid. The temperature was chosen to be so close to the melting point as possible. Temperature cycling, simulating the cooling/heating cycles, was used. The liquid was solidified by cooling it down to 293.15 K. The total time of the cycling experiments was 1179 hours, in which a liquid state was maintained for 664 hours. The weight losses were measured roughly 0.5 hour before the cooling. The aluminium samples were quickly taken out, flushed with deionized water, and dried at 353.15 for 30 minutes followed by weighting, an accuracy of 0.05 mg, and returning back to the flasks.

After the corrosion experiments the samples were treated as described above, subsequently they were analysed by XRD (STOE P, Bruker), and SEM (Carl Zeiss EVO 40, Germany). Corrosion products were removed according to the ISO 8407 by immersing the corroded samples into nitric acid for 5 minutes, followed by flushing with deionized water dried at 353.15 K for 30 minutes, and weighed to calculate the total corrosion loss.

3. Results and discussion

Calorimetric experiments

Supercooling is a common issue of PCMs, and can also be observed during repeated charge-discharge cycles of MNH [2]. Large supercooling and thermal instability of MNH is evident in Fig. 1, which shows DSC traces of 1st, 30th, 60th and 75th cycles of heating and cooling. Two endothermic peaks corresponding to solid-solid {(s)-(s)} phase transition, and melting are observed during the heating scan, unlike only one sharp peak, or one peak with indication of blending of two effects, is detected on cooling. DSC traces were evaluated as a sum of the both contributions during heating ($\Delta H_h=\Delta_{fus}H+\Delta_{tr}H$), and cooling ($\Delta H_c=\Delta_{cr}H+\Delta_{tr}H_{(c)}$) scans allowing comparing absorbed and released heats, where ΔH_h is the total enthalpy change on heating, $\Delta_{tr}H$ is the enthalpy of the (s)-(s) transition; ΔH_c is the sum of the enthalpy of crystallization, $\Delta_{cr}H$, and the enthalpy of (s)-(s) transition, $\Delta_{tr}H_{(c)}$, on

cooling. The melting process is very reproducible and stable with average values of T_m = 361.9±0.1 K, and ΔH_h = 153.8±0.5 J g^{-1} for all 75 cycles. Crystallization shows almost constant values of ΔH_c = −140.3±1.9 J g^{-1}, but large fluctuation in T_{cr}, the average value of T_{cr} = 334.9±4.1 K over 75 cycles (Fig. 2). The average value of supercooling is as large as ΔT = 27.0±4.1 K.

Promising nucleating agents from the group of non-isostructural nucleating agents were selected from Lane's work [2], and their long-term use for suppressing the supercooling in mixtures with MNH is studied. The list of all tested nucleating agents with values of T_m, T_{cr}, ΔH_h, ΔH_c, and ΔT averaged from 2nd, 3rd, and 4th measured cycles are shown in Table 1, and graphically presented in Figure 3.

The results clearly show that all tested carbonates, except of $MgCO_3$ do not supress supercooling, and the addition of AlO(OH) does not provide acceptable suppression. The addition of BaO_2 decreases supercooling below 3 K but the value of the enthalpies change is significantly reduced which makes BaO_2 unsuitable for effective heat accumulation.

The evaluation of the promising nucleating agents is made on the basis of comparing simultaneously supercooling and the enthalpy results; BaO, $Ba(OH)_2.8H_2O$, MgO, $Mg(OH)_2$, $MgCO_3$, or $Sr(OH)_2$ additives are identified as the most promising agents with significant suppression of supercooling, and negligible changes in the enthalpy values. These compounds were subsequently tested in 0.5, 1 and 2 wt% additions to MNH during 50 charge/discharge cycles. The determined averaged values of melting/crystallization temperatures, and enthalpy changes over 50 cycles are summarized in Table 2, and graphically shown in Figure 4 together with the values of supercooling.

The heating/cooling 50 cycles reveal differences in behaviour of the six promising nucleating agents. Two salts ($Ba(OH)_2.8H_2O$ and $MgCO_3$) have to be excluded because significant increase in supercooling during the long-term tests. None of the tested carbonates is optimal as a nucleating agent for MNH. On the other hand, the last four from the promising group of Figure 4 seem to be very good candidates as nucleating agents. The most effective is $Mg(OH)_2$ with smallest supercooling, and high enough stable enthalpy (Fig. 4). In the case of BaO, MgO and $Sr(OH)_2$ we observe increase in supercooling for mixtures with 2 wt. % of the agent addition. Dependence of the supercooling for the four favourite salts, $Mg(OH)_2$, MgO, BaO, and $Sr(OH)_2$, during 50 cycles is shown in Fig. 5. It is evident that $Mg(OH)_2$ is stable for all 50 cycles, and the supercooling is less than 4 K for all concentrations studied (Fig. 5a). In the case of 2 wt% MgO (Fig. 5b), we observe increase in supercooling after the 15th cycle, but for the lower concentrations of the nucleating agent the supercooling of 3.4 K is comparable to $Mg(OH)_2$. The repeated heating/cooling cycles of MNH with BaO show increase in supercooling from 30th cycle, or sooner when the concentration of BaO in the mixture is higher (Fig. 5c). Very good suppression of supercooling is achieved with lower addition of $Sr(OH)_2$, ΔT ~3.5 K, with gradual decrease to 0 K after 25th thermal cycle for 1 wt. % mixture (Fig. 5d). The addition of nucleating agents influences both the position and the shape of DSC peaks as it is shown in Fig. 6 (mixture of MNH with 0.5 wt% $Mg(OH)_2$). Commonly, the crystallization peaks become broader with lower heat flow than those observed for pure MNH and for mixtures during the1st cycle. For better approximation of natural temperature conditions, heating rate of 2 K min^{-1} is used for the pure MNH and MNH+0.5 wt% $Mg(OH)_2$. The slow heating rate results in ΔT = 18 K for pure MNH (2–4 cycle). At the same conditions, MNH+0.5 wt% $Mg(OH)_2$ shows decrease in supercooling to ΔT = 2.4 ± 0.1 K. Therefore the slower heating rate, simulating the common weather conditions, has positive effect on nucleation.

Considering the low concentration of the nucleating agent, the heat capacity of the nucleating agent can be neglected because of its low concentration. The amount of the stored

heat, Q_p, in PCM during heating can be estimated from room temperature up to T_m using the heat capacity polynomial functions [7], and the enthalpy of MNH determined from measurements of MNH mixtures, according to:

$$Q_p = \int_{298.15}^{T_{tr}} c_{ps_1}.dT + \Delta_{tr}H + \int_{T_{tr}}^{T_m} c_{ps_2}.dT + \Delta_{fus}H$$
$$= c_{ps_1}.(T_{tr} - 298.15) + \Delta_{tr}H + + c_{ps_2}.(T_m - T_{tr}) + \Delta_{fus}H \quad (1)$$

where $\Delta_{tr}H$ is the enthalpy of (s)-(s) and $\Delta_{fus}H$ is the enthalpy of (s)-(l) phase transitions (both in J g^{-1}). The specific heat capacities c_{ps_1}, c_{ps_2} and c_{pl} are given in J g^{-1} K^{-1} for the solid-s_1, the solid-s_2, and the liquid phases, respectively. The enthalpy of the phase transition plays significant role in energy storage. However, the contribution of the heat capacity covers about 31% of the storing capacity of the studied mixtures. The published stored heat of pure MNH during the first heating cycle is 248.8 J g^{-1} [7], and it varies with the nucleating agent being used from 208 J g^{-1} (2 wt% MgO) to 226 J g^{-1} (0.5 wt% BaO) of the accumulated heat energy based on the average values of enthalpies over 2-50 cycles.

Corrosion tests

In the previous part, the perspective candidates for nucleating agents in magnesium nitrate hexahydrate have been identified. From the practical application point of view it is necessary to known the corrosive properties of pure MNH, and its mixtures containing the nucleating agents. To maintain the highest heat storage possible and the lowest supercooling, concentration of 0.5 wt% of nucleating hydroxides $Mg(OH)_2$ and $Sr(OH)_2$ has been chosen for corrosion tests and compared with pure MNH. The temperature regime simulating the cooling/heating cycles where each process of heating/melting and solidification/cooling has taken one hour is schematically shown in Figure 7, and the corresponding measured mass losses are shown in Figure 8. The mass of the aluminium samples in MNH medium slightly decreases at the beginning of the test, and then remains approximately constant. When magnesium hydroxide is added to MNH, the sample mass markedly increases after 500 hours of the corrosion test. On the other hand, when strontium hydroxide is added, the sample mass remains unchanged. This different behaviour is also visible on the surface of the samples (Fig. 9a –c), and in the corrosion potentials (Tab. 3).

According to the Pourbaix diagram [22], the aluminium should be in the state of passivity at the conditions under study. Change of the corrosion potential in pure MNH indicates low dissolution of aluminium, which is in agreement with the mass changes in Figure 8. A compact layer of corrosion products is not developed on the surface, which is only partially covered with the corrosion products, originating, probably, from impurities in the aluminium alloy (Fig. 9a). The aluminium alloy contains 0.5 wt% of manganese. When $Mg(OH)_2$ is added into MNH, the corrosion potential is significantly shifted into negative values. This means aluminium dissolution, and a layer of corrosion products is formed on the surface (Fig. 9b). The surface corrosion layer contains cracks, and does not form a compact barrier which would prevent contact with the solution (Fig. 9d). In the case of $Sr(OH)_2$ as the additive, the corrosion potential shifts to more positive values indicating passivation of the aluminium alloy surface. The compact layer forms a barrier that prevents contact with the solution (Fig. 9c). This is in agreement with the observed mass changes in Figure 8.

The corrosion products were removed according to the ISO 8407, after the corrosion tests, and the corrosion rate was calculated. The corrosion rate was calculated using the total time of in the molten salt, and the results are presented in Table 3. It can be seen that the corrosion rate of the aluminium alloy is low, 2.3–3.0 mg cm^{-2} $year^{-1}$. Corrosion is effectively

inhibited, which is in accordance with the Pourbaix diagram [22]. The differences in the corrosion rates in Table 3 are not significant. Guideline for corrosion weight loss used in industry can be found in Refs. [21, 23, 24]. It follows that aluminium alloy can be used as a construction material for long-term operations. The obtained results are in good agreement with Nagano *et al.* [20], who studied corrosion of aluminium alloy in NMH with the addition of $MgCl_2$.

Conclusions

The thermal stability of pure magnesium nitrate hexahydrate was studied during 75 heating and cooling cycles, and supercooling of about 27 K is found. Therefore, the non-isostructural nucleating agents were added into MNH in 1 wt%, and tested during 4 cycles. This fast testing identified the most promising salts as the nucleating agents, which were then tested for 50 thermal cycles in the addition of 0.5, 1 and 2 wt% of the nucleating agent. The most effective nucleating agents are $Mg(OH)_2$ in the additions of 0.5–2 wt%, and BaO, MgO or $Sr(OH)_2$ in the amount of 0.5–1 wt%. The corrosion tests of MNH, and MNH with 0.5 wt% of $Mg(OH)_2$ or $Sr(OH)_2$ confirm the aluminium alloy as a suitable, and sufficiently resistant material for the heat storage containers.

Acknowledgment

This work was supported by courtesy of the Slovak Grant Agency (VEGA 1/0101/14).

References

[1] Zalba B, Marín JM, Cabeza LF, Mehling H. Review on thermal energy storage with phase change: material, heat transfer analysis and applications. Appl Therm Eng. 2003;23:251–83.

[2] Lane GA. Low temperature heat storage with phase change materials. Int. J. Ambient Energy 1980;1:155–68.

[3] Lane GA. Phase change materials for energy storage nucleation to prevent supercooling. Sol Energy Mater Sol Cells 1992;27:135–60.

[4] Cantor S. Applications of differential scanning calorimetry to study of thermal-energy storage. Thermochim Acta 1978;26:39–47.

[5] Cantor S. DSC study of melting and solidification of salt hydrates. Thermochim Acta. 1979;33:69–86.

[6] Naumann R, Emons HH, Köhnke K, Paulik J, Paulik F. Investigation on thermal behaviour of $Mg(NO_3)_2 \cdot 6H_2O$. J Therm Anal. 1988;34:1327–1333.

[7] Sadovska G., Honcova P, Pilar R, Calorimetric study of calcium nitrate tetrahydrate and magnesium nitrate hexahydrate. J Therm Anal. 2016;124:539–546.

[8] Lorsch GH, Kauffman KW, Dentons JC. Thermal energy storage for solar heating and off-peak air conditioning. Energ Convers. 1975;15:1–8.

[9] Voigt W, Zeng D. Solid-liquid equilibria in mixtures of molten salt hydrates for the design of heat storage materials. Pure Appl Chem. 2002;74:1909–1920.

[10] Guion J, Sauzade JD, Laügt M. Critical examination and experimental determination of melting enthalpies and entropies of salt hydrates. Thermochim Acta. 1983;67:167–179.

[11] Naumann R, Emons HH. Results of thermal analysis for investigation of salt hydrates as latent heat-storage materials. J Therm Anal. 1989;35:1009–1031.

[12] Sharma A, Tyagi VV, Chen CR, Buddhi D. Rewiev on thermal energy storage with phase change materials. Renew Sust Energ Rev. 2009;13:318–345.

[13] Riesenfeld EH, Milchsack C. Versuch einer Bestimmung des Hydratationsgrades von Salzen in koncentrierten Lösungen. Z Anorg Chem. 1914;85:401−429.
[14] Demirbas MF. Thermal energy storage and phase change materials: An overview. Energ Source Part B. 2006;1:85-95.
[15] Nagano K, Ogawa K, Mochida T, Hayashi K, Ogoshi H. Thermal characteristics of magnesium nitrate hexahydrate and magnesium chloride hexahydrate mixture as a phase change material for effective utilization of urban waste heat. Appl Therm Eng. 2004;4:221–32.
[16] Zhdanov VM, Shamova VA, Drakin SI. Heat capacity of crystal hydrates of magnesium, aluminum, calcium, nickel, and lanthanum nitrates and copper sulfate pentahydrate. Deposited Doc. VINITI. 1976;2874-76:1−10.
[17] Yaws, Carl L. Heat Capacities of Solids - Elements and Inorganic Compounds In: Yaws' Handbook of Thermodynamic Properties for Hydrocarbons and Chemicals. Knovel. 2009.
http://app.knovel.com/hotlink/toc/id:kpYHTPHC09/yaws-handbook-thermodynamic/yaws-handbook-thermodynamic. Accessed 31 March 2009.
[18] Cabeza LF, Illa J, Roca J, Badia F, Mehling H, Hiebler S, Ziegler F. Immersion corrosion tests on metal-salt hydrate pairs used for latent heat storage in the 32 to 36 degrees C temperature range. Mater Corros 2001;52:140–6.
[19] Cabeza LF, Illa J, Roca J, Badia F, Mehling H, Hiebler S, Ziegler F. Middle term immersion corrosion tests on metal-salt hydrate pairs used for latent heat storage in the 32 to 36 degrees C temperature range. Mater Corros 2001;52:748–54.
[20] Nagano K, Ogawa K, Mochida T, Hayashi K, Ogoshi H. Thermal characteristics of magnesium nitrate hexahydrate and magnesium chloride hexahydrate mixture as a phase change material for effective utilization of urban waste heat. Appl Therm Eng 2004;24:209–20.
[21] Moreno P, Miró L, Solé A, Barreneche C, Solé C, Martorell I, Cabeza LF. Corrosion of metal and metal alloy containers in contact with phase change materials (PCM) for potential heating and cooling applications. Appl Energy 2014;125:238–45.
[22] Wranglén G. An Introduction to Corrosion and Protection of Metals. Stockholm: Institut for Metallskydd, Fack 10041; 1972.
[23] Cabeza LF, Svensson G, Hiebler S, Mehling H. Thermal performance of sodium acetate trihydrate thickened with different materials as phase change energy storage material. Appl Therm Eng 2003;23:1697–704.
[24] Davis JR. Corrosion – understanding the basics. 1st ed. Ohio: ASM, International; 2000.

Table 1 Thermodynamic data obtained from thermal stability test of pure MNH, and its mixtures with 1 wt% of nucleating agents: T_m – the melting temperature; ΔH_h – the sum of the enthalpy change of fusion and (s)-(s) transformation during heating ($\Delta_{fus}H+\Delta_{tr}H$) ; T_{cr} – the temperature of crystallization; ΔH_c – the sum of the enthalpy change of crystallization and (s)-(s) transformation during the cooling ($\Delta_{cr}H+\Delta_{tr}H_{(c)}$); ΔT - supercooling ($T_m - T_{cr}$). All values represent averages of 2–4 cycles.

nuc. agent	T_m/K	ΔH_h/J g^{-1}	T_{cr}/K	ΔH_c/J g^{-1}	ΔT/K
none	361.8±0.1	153.3±0.3	333.3±3.9	–139.9±2.0	28.5±3.9
AlO(OH)	363.6±0.1	149.0±0.8	352.5±5.9	–146.4±6.0	11.1±5.9
BaO	362.8±0.1	148.3±0.8	359.5±0.4	–147.9±0.8	3.3±0.4
BaO_2	361.7±1.7	120.4±25.0	359.5±0.7	–106.3±19.8	2.2±0.9
$Ba(OH)_2.8H_2O$	362.2±0.1	142.9±0.1	359.1±0.3	–146.1±0.1	3.1±0.2
$BaCO_3$	362.2±0.1	140.9±2.8	339.1±5.8	–133.0±8.3	23.1±5.8
CaO	359.2±0.4	106.8±2.1	352.0±1.9	–123.5±1.8	7.2±2.2
$Ca(OH)_2$	360.7±0.2	133.8±1.9	354.7±2.1	–140.6±1.3	6.0±2.3
$CaCO_3$	362.8±0.1	148.6±0.6	338.8±10.7	–129.2±16.6	24.0±10.7
MgO	363.3±0.1	150.1±0.3	359.9±0.2	–150.5±0.5	3.4±0.2
$Mg(OH)_2$	362.8±0.2	144.4±0.7	359.4±0.2	–145.1±0.4	3.3±0.1
$MgCO_3$	363.6±0.1	159.9±1.0	358.9±0.8	–159.5±0.4	4.7±0.8
$Sr(OH)_2$	361.1±0.1	151.5±1.8	356.2±2.2	–153.0±1.0	4.9±2.2
$SrCO_3$	360.9±0.1	133.2±0.2	333.5±3.8	–133.9±5.1	27.4±3.9

Table 2 Thermodynamic data obtained from thermal stability test of MNH, and its mixtures with nucleating agents (the amount of the agent in the mixture is between 0.5–2 wt%) during 2-50 cycles

nuc. agent /wt%		T_m /K	ΔH_h/J g^{-1}	T_{cr} /K	ΔH_c/J g^{-1}	ΔT/K
none	—	361.8±0.1	153.7±0.4	333.5±3.4	−139.9±1.5	28.3±3.4
BaO	0.5	363.3±0.1	148.8±2.0	358.7±1.5	−148.5±0.5	4.6±1.5
	1	362.8±0.1	148.3±0.8	359.5±0.4	−147.9±0.8	3.3±0.4
	2	362.6±0.1	131.7±1.4	355.1±3.5	−134.5±1.0	7.5±3.6
$Ba(OH)_2.8H_2O$	0.5	363.5±0.1	139.1±1.4	356.6±1.8	−143.9±1.5	6.9±1.8
	1	362.0±0.1	134.3±2.0	354.7±1.7	−139.2±1.6	7.3±1.7
	2	359.5±1.2	92.9±4.0	349.3±0.8	−111.2±3.0	10.2±1.3
MgO	0.5	363.5±0.1	147.8±1.4	360.4±0.2	−147.7±1.4	3.0±0.1
	1	363.4±0.1	143.6±2.1	360.2±0.2	−144.7±1.3	3.2±0.1
	2	362.5±0.2	124.4±4.0	356.3±1.7	−131.6±1.5	6.1±0.8
$Mg(OH)_2$	0.5	361.7±0.1	140.4±0.4	358.1±0.2	−139.9±0.4	3.5±0.2
	1	362.8±0.1	138.9±2.8	359.5±0.3	−141.7±1.9	3.2±0.3
	2	361.1±0.1	138.3±2.3	358.1±0.2	−137.8±1.7	2.9±0.2
$MgCO_3$	0.5	363.7±0.1	155.6±1.2	344.7±8.5	−140.1±41.3	19.0±8.5
	1	363.5±0.1	157.2±1.7	351.5±5.9	−151.5±11.9	11.9±5.9
	2	363.9±0.1	157.1±2.9	346.9±12.6	−143.2±14.9	17.0±12.5
$Sr(OH)_2$	0.5	360.1±0.1	139.0±0.7	356.8±0.5	−141.6±0.5	3.2±0.5
	1	360.8±0.1	144.3±2.9	357.2±1.4	−146.1±2.5	3.6±1.4
	2	358.8±0.1	130.0±1.9	350.6±1.1	−132.2±2.0	7.3±1.2

Table 3 Potential of hydrogen, pH, of the liquid phase, corrosion potentials, *E*, and the corrosion rate of aluminium alloy in the studied PCMs. $E_{corr,start}$, $E_{corr,end}$ are the corrosion potentials at the beginning and the end of the corrosion test, respectively

PCM	**pH**	$E_{corr,start}$ **/V vs. SCE**	$E_{corr,end}$ **/V vs. SCE**	**Corrosion rate /mg cm^{-2} year^{-1}**
MNH	6.5	–0.521	–0.589	2.9
MNH + 0.5 wt% $Mg(OH)_2$	7.0	–0.644	–0.863	3.0
MNH + 0.5 wt% $Sr(OH)_2$	7.5	–0.467	–0.326	2.3

List of figures

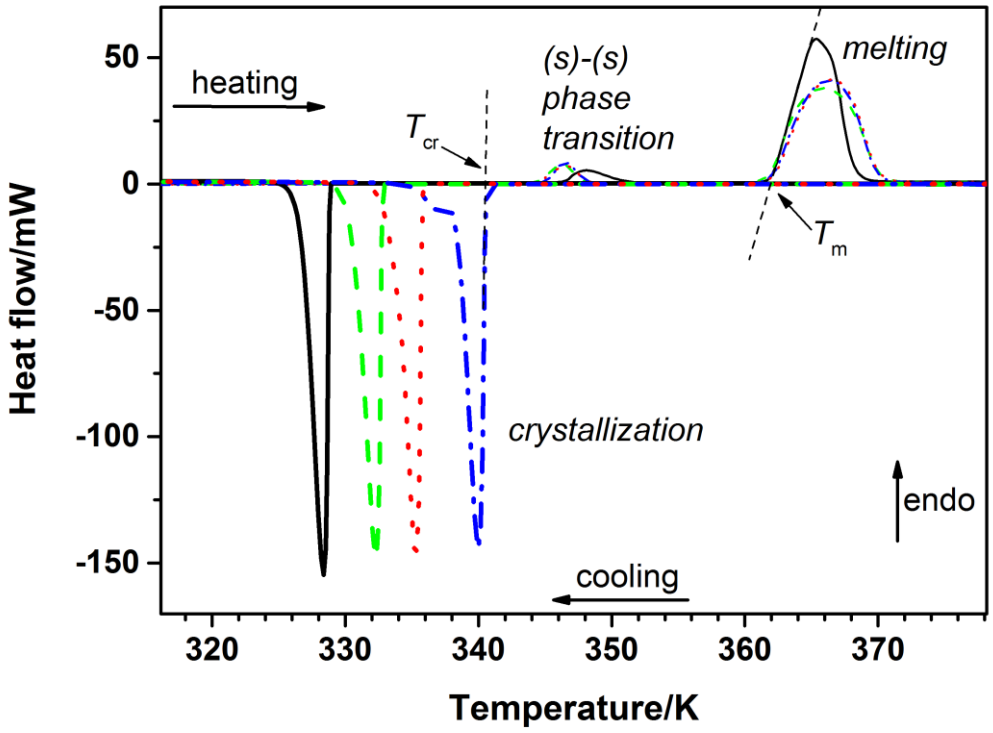
heating
T_{cr}
(s)-(s)
phase
transition
melting
T_m
crystallization
endo
cooling
Heat flow/mW
Temperature/K
50
0
-50
-100
-150
320
330
340
350
360
370

Fig. 1

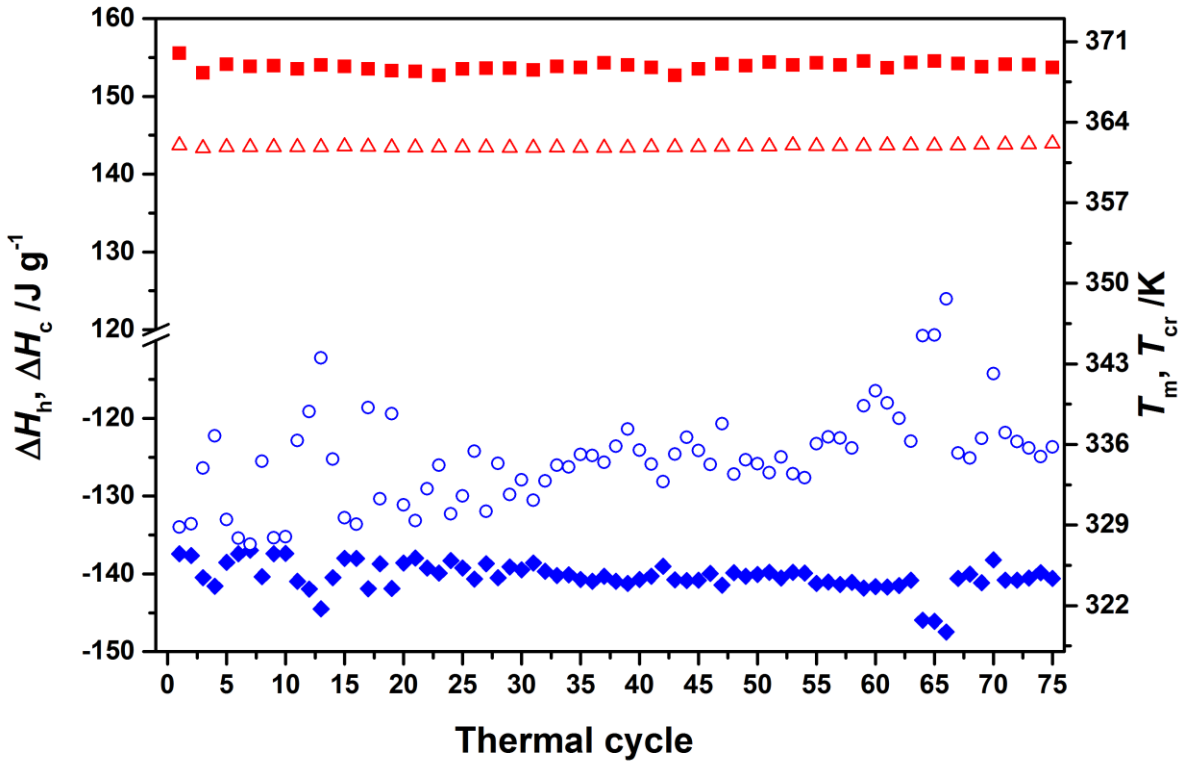
ΔH_h, ΔH_c /J g^{-1}
T_m, T_{cr} /K
Thermal cycle
160
150
140
130
120
-120
-130
-140
-150
371
364
357
350
343
336
329
322
0
5
10
15
20
25
30
35
40
45
50
55
60
65
70
75

Fig. 2

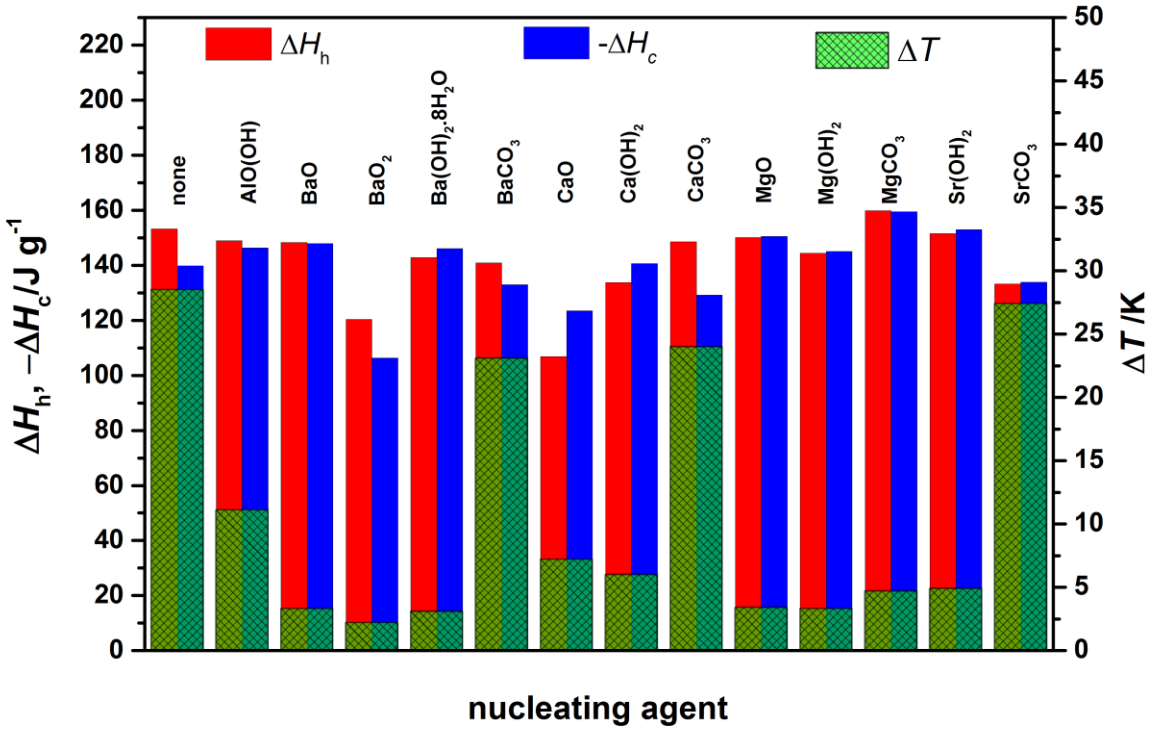
ΔH_h
-ΔH_c
ΔT
none
AlO(OH)
BaO
BaO2
Ba(OH)2·8H2O
BaCO3
CaO
Ca(OH)2
CaCO3
MgO
Mg(OH)2
MgCO3
Sr(OH)2
SrCO3
ΔH_h, −ΔH_c /J g-1
ΔT /K
nucleating agent

Fig. 3

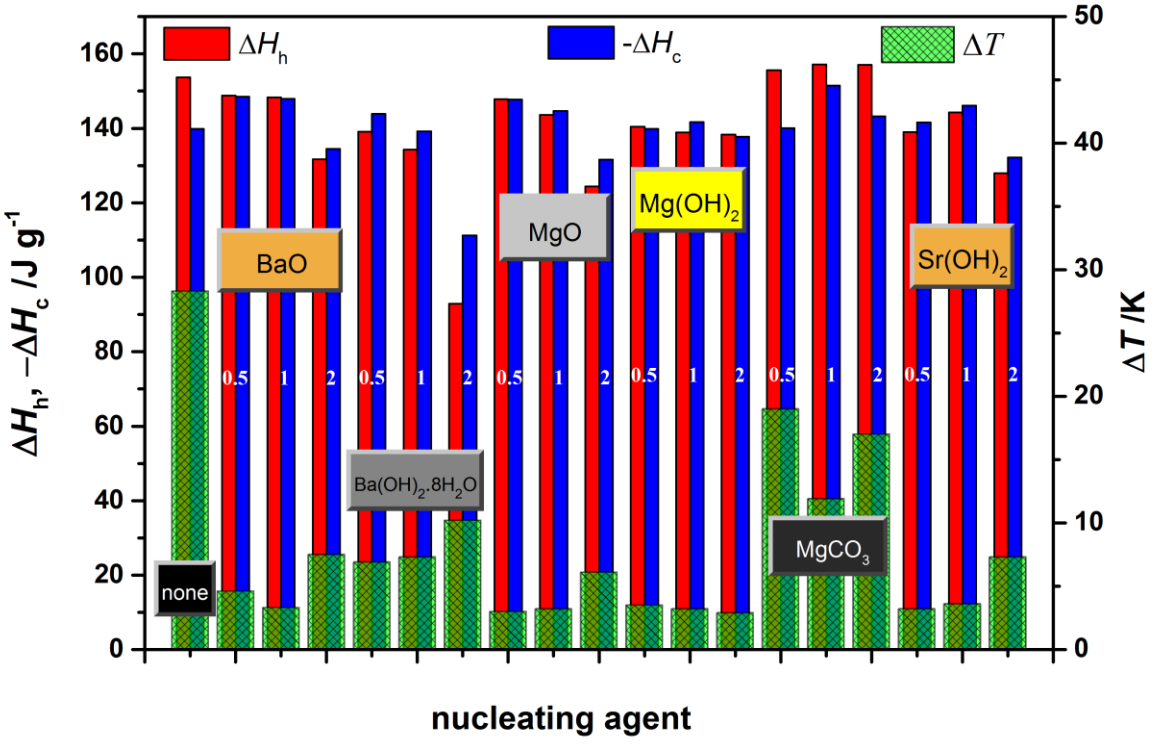
ΔH_h
-ΔH_c
ΔT
none
BaO
Ba(OH)2·8H2O
MgO
Mg(OH)2
MgCO3
Sr(OH)2
0.5
1
2
ΔH_h, −ΔH_c /J g-1
ΔT /K
nucleating agent

Fig. 4

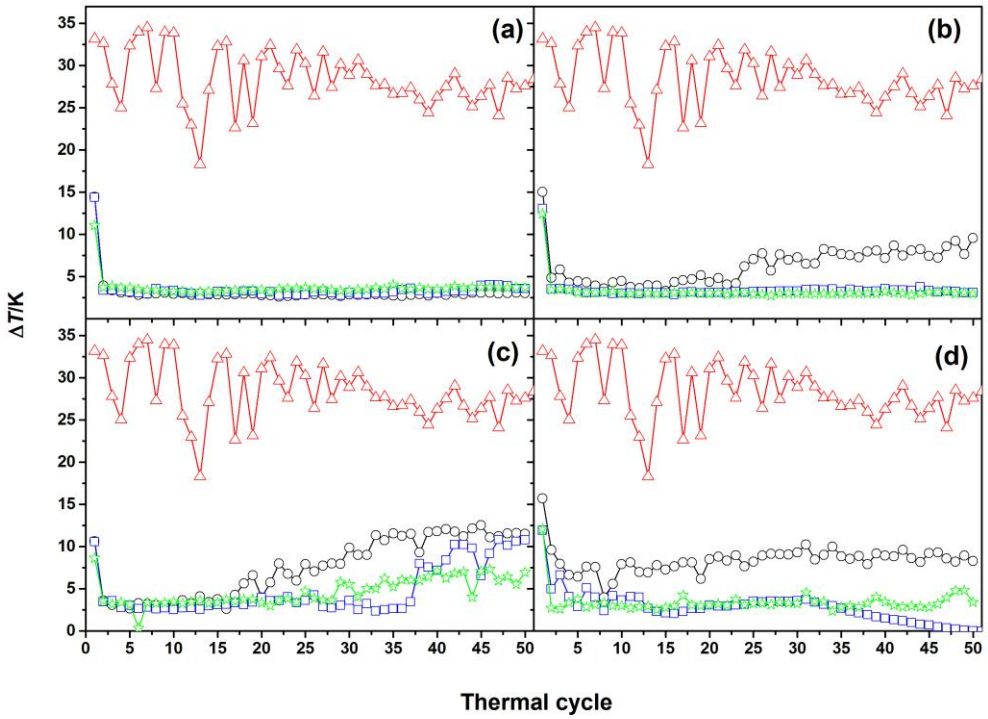
(a)
(b)
(c)
(d)
ΔT/K
Thermal cycle

Fig. 5

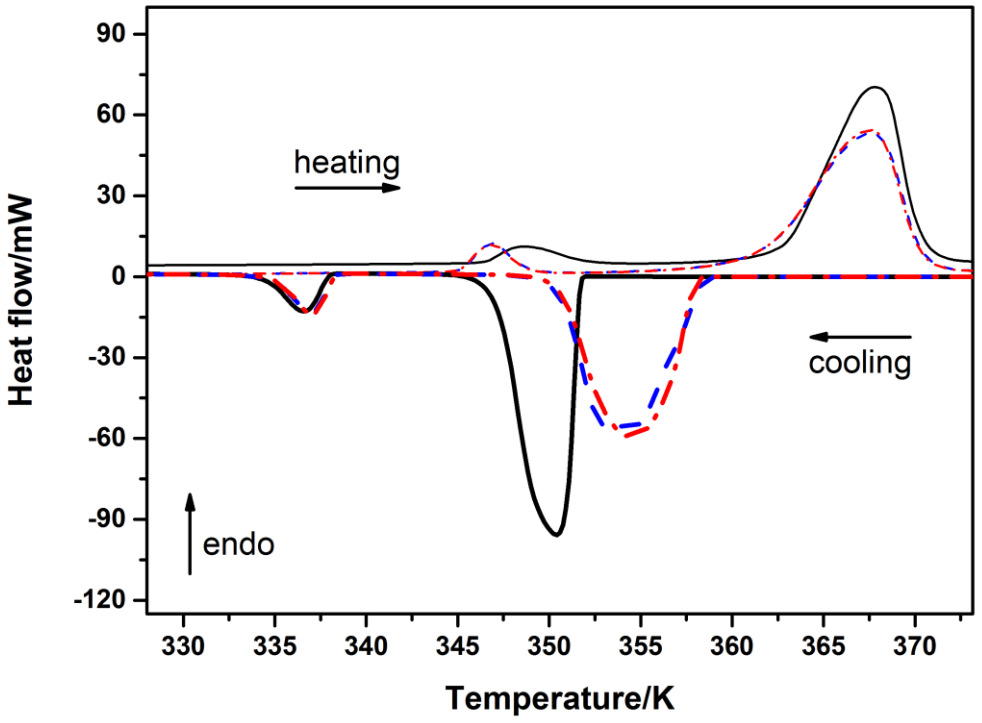
heating
cooling
endo
Heat flow/mW
Temperature/K

Fig. 6

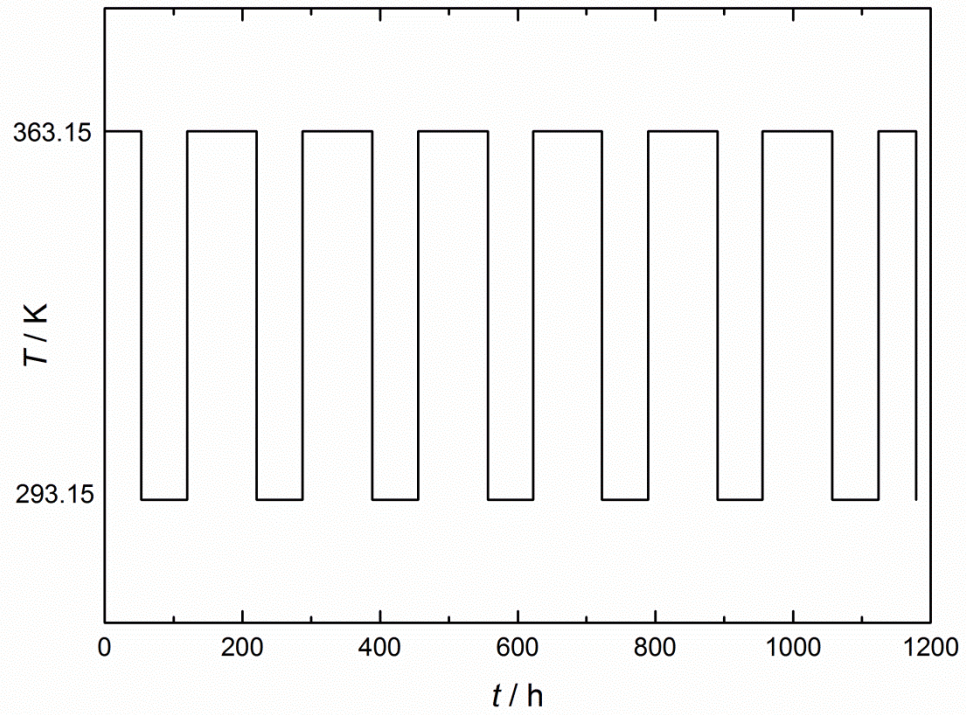
363.15
293.15
T / K
0
200
400
600
800
1000
1200
t / h

Fig. 7

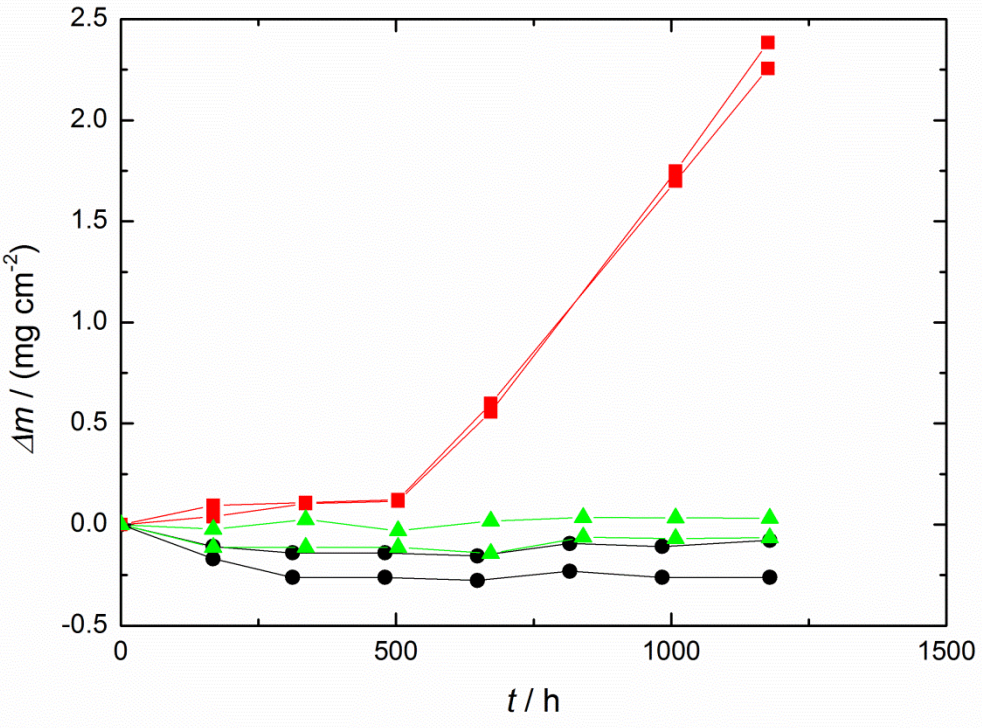
2.5
2.0
1.5
1.0
0.5
0.0
-0.5
Δm / (mg cm-2)
0
500
1000
1500
t / h

Fig. 8

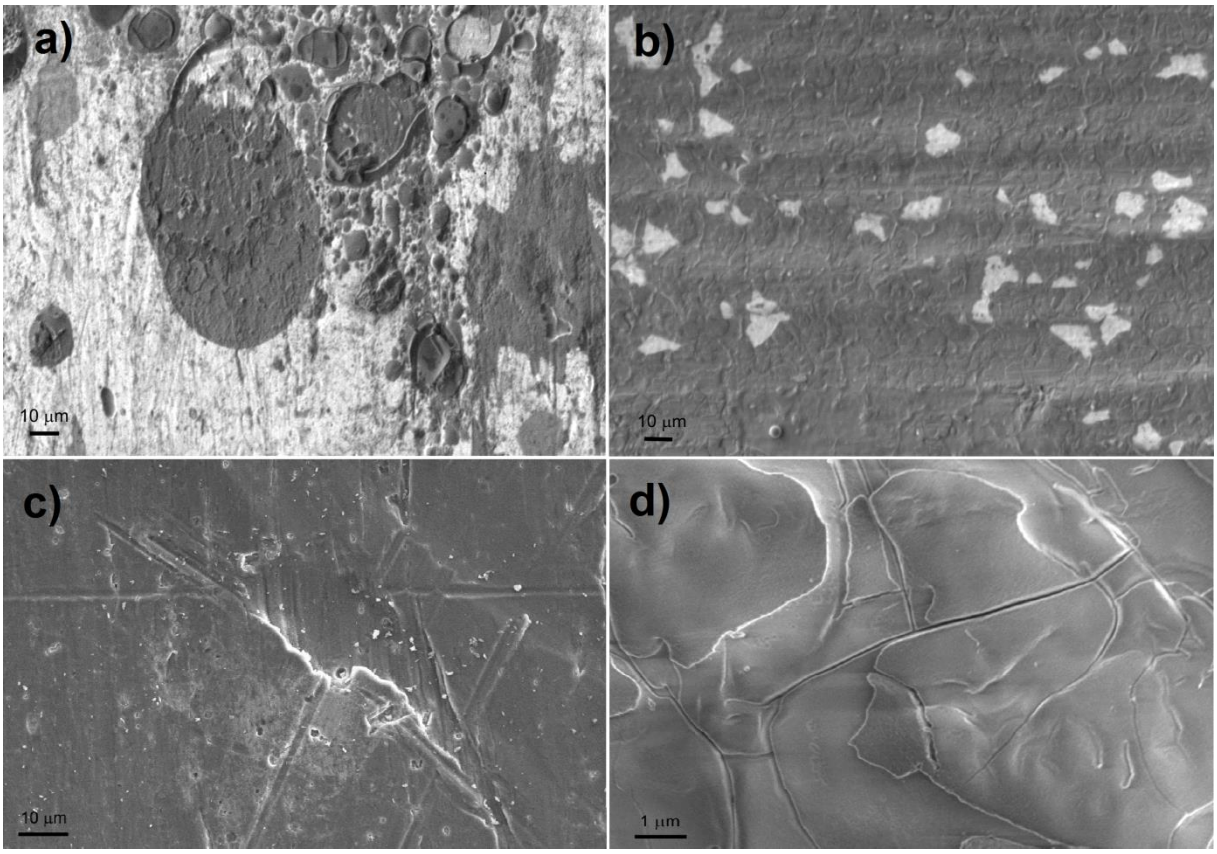

Fig. 9